Electrostatic Stabilization in Methionine Aminopeptidase from Hyperthermophile *Pyrococcus furiosus*[†]

Kyoko Ogasahara,[‡] Elena A. Lapshina,[‡] Miyo Sakai,[‡] Yukiko Izu,[§] Susumu Tsunasawa,[§] Ikunoshin Kato,[§] and Katsuhide Yutani*[,‡]

Institute for Protein Research, Osaka University, 3-2 Yamadaoka, Suita City, Osaka 565-0871, Japan, and Biomedical Group, Takara Shuzo Co. Ltd., Seta, Ohtsu City, Shiga 520-21, Japan

Received December 29, 1997; Revised Manuscript Received March 6, 1998

ABSTRACT: The thermostability of methionine aminopeptidase from a hyperthermophile *P. furiosus* (*Pf*MAP) was extremely high: the denaturation temperature was 106.2 °C at pH 10.2. To explore the contribution of electrostatic interaction to the superior thermostability of *Pf*MAP, the thermostability of *Pf*MAP was examined by differential scanning calorimetry (DSC) in various salt concentrations in the acidic region far from the isoelectric point of *Pf*MAP. (1) In 20 mM glycine buffer, the DSC curve of *Pf*MAP exhibited a single peak. Transition temperatures (T_m) were lowered with decreasing pH from 4 to 3. The heat denaturation of *Pf*MAP was not reversible. (2) Denaturation enthalpy (ΔH) measured at different pHs linearly correlated with T_m up to 102 °C, suggesting that the denaturation heat capacity (ΔC_p) for *Pf*MAP is constant up to 100 °C. ΔC_p was estimated to be 0.82 J K^{-1} g^{-1}. (3) In the presence of 10−100 mM KCl at pH 3.2, two peaks appeared on the DSC curves. The first peak shifted to lower temperatures with increasing concentration of KCl and, oppositely, the second one to higher temperatures. It was found that the first and second peaks originated from the heat denaturation of the native form of *Pf*MAP and the melting of the non-native associated form having molten globule-like structure, respectively, judged from the CD spectra and ultracentrifugation analyses. This indicates the following: first, the attractive electrostatic interaction is an important factor in stabilizing the native form of *Pf*MAP; second, the presence of KCl stimulates the formation of the molten globule-like state of *Pf*MAP and stabilizes it. (4) In a comparison of the sequence and crystal structure of *Pf*MAP, which has been recently determined (1xgs.pdb), with those of MAP from *Escherichia coli* (*Ec*MAP), it was predicted that the extra four short-range ion pairs less than 3 Å involved in *Pf*MAP are crucial candidates as determinants for the superior thermostability of *Pf*MAP.

Many novel hyperthermophiles, which can grow preferentially at extremely high temperatures near the boiling point of water, have been isolated in the vicinity of both terrestrial and submarine geothermal environments (*1*−*4*). The majority belongs to the phylogenetical domain of Archaea (*5*). Hyperthermophilic organisms have provided intriguing subjects in biological science: evolution of life, adaptation of life to high temperature, features of the metabolism and the materials constituting the cell. Especially among them, understanding the functional and structural properties of proteins from hyperthermophiles should provide important clues as to how hyperthermophiles can be alive under conditions where normal proteins denature, because proteins are key molecules which carry out the most essential and fundamental tasks in living organisms. The results on several proteins reported have revealed that purified proteins from hyperthermophiles maximally exhibit enzymatic activities near 100 °C and denature at unusually high temperatures. One of the fundamental questions on the molecular level of the strategies for these high-temperature adaptations concerns the structural and energetic basis of protein stability at an extremely high temperature. Elucidating the mechanism stabilizing hyperthermophile proteins is not only itself a great challenge but also provides valuable insight into understanding the mechanisms of conformational stabilization and protein folding for general proteins, which is now one of the important problems in biological science (*6*). Moreover, finding the origin of the extraordinary thermal stability of proteins from hyperthermophiles opens a great advantage in biotechnological applications. It could lead us how to create the desired proteins with higher stability or activity at elevated temperatures.

To date, the three-dimensional structures for several proteins from hyperthermophiles have been determined, and the factors responsible for high conformational stabilities have been discussed (*7*−*14*). However, it is not known whether there is a common mechanism responsible for the extra stability of proteins from hyperthermophiles. The mechanism attributed to the hyperthermostability of a protein remains to be resolved. Detailed studies on the molecular level on the stability of hyperthermophile proteins have recently just started.

[†] This work was supported in part by a Grant-in-Aid (07280103) for Scientific Research from the Ministry of Education, Science and Culture of Japan to K.Y.

* To whom all correspondence should be addressed. Phone: 81-6-879-8615. Fax: 81-6-879-8616. E-mail: yutani@protein.osaka-u.ac.jp.

[‡] Osaka University.

[§] Takara Shuzo Co. Ltd.

S0006-2960(97)03172-3 CCC: $15.00
Published on Web 04/11/1998

To explore the determinants responsible for the extraordinary stability of proteins from hyperthermophilic organisms, we have chosen methionine aminopeptidase (MAP)[1] (EC 3.4.11.18) from a hyperthermophilic archaeon, *Pyrococcus furiosus*, which grows optimally at about 100 °C (*15*). MAP is a Co^{2+}-dependent peptidase and catalyzes the removal of N-terminal methionine. Protein synthesis is initiated with either *N*-formylmethionine or methionine. The N-formyl group or methionine of nascent polypeptide is removed by deformylase or MAP, respectively, resulting in mature proteins without amino-terminal leader methionine residue. MAP plays a role in the post-translation of proteins after biosynthesis and is isolated from various organisms from bacteria to human (*16*−*18*). Depending on the sequences, MAP can been classified into two types: type 1 is the prokaryotic form, and type 2 the eukaryotic one. The eukaryotic type has an extra long insertion sequence of approximately 60 residues compared with those from the prokaryotic type and a variable N-terminal extension (*18*, *19*). MAP from *P. furiosus* (*Pf*MAP) is composed of 295 amino acid residues (molecular weight = 32.74 K) and involves an extra insertion of 62 residues in comparison with MAP from *E. coli* (*Ec*MAP), indicating that *Pf*MAP belongs to the eukaryotic type (*20*).

The gene of *Pf*MAP has been transformed into *Escherichia coli*, and the general properties have been examined (*20*). *Pf*MAP exhibits the maximum activity at 90 °C in the presence of Co^{2+} and is stable against heat and chemical denaturants; the activity is completely retained after heating at 75 °C for 60 min over the pH range 4.5−10.5, and loss of activity is not observed at all under incubation with a buffer (pH 7.5) containing ether 0.01% SDS or 8 M urea at 37 °C for 1 h. *Pf*MAP exists as a monomer and has no Cys. The numbers (the ratio %) of Glu and Lys in *Pf*MAP are 30 (10.2%) and 26 (8.8%), respectively. On the contrary, there are 22 (8.3%) and 18 (6.8%) in *Ec*MAP, respectively (*16*). The high contents of Glu and Lys in *Pf*MAP seem to suggest the contribution of a salt bridge to the stability of *Pf*MAP. Perutz and Radit (*21*, *22*) have early proposed the contribution of a salt bridge to the high thermal stability of ferredoxin from thermophile from the sequence comparisons between homologues from thermophilic and mesophilic organisms. Several proteins from hyperthermophiles have been recently reported to have tremendous increases in ion pair content (*7*−*13*).

In this study, focusing on the electrostatic interaction as determinant in stabilizing *Pf*MAP, we examined the effect of salt on the thermal stability of *Pf*MAP using differential scanning calorimetry (DSC) at various pHs. Since the X-ray crystal structure of *Pf*MAP has just been determined (1xgs.pdb, personal communication from Tahirov et al.),[2] the forces attributed to the extraordinary thermostability of *Pf*MAP were explored on the bases of the present experimental results and the three-dimensional structure in comparison with the structure of *Ec*MAP, which has been already determined by Roderick and Matthews (*23*). It will be discussed that the electrostatic interaction is an important factor stabilizing *Pf*MAP.

MATERIALS AND METHODS

Protein Expression and Purification. *Pf*MAP was expressed in *E. coli* strain JM109/pMap8 cloning the *Pf*MAP gene (*20*). The *E. coli* strain JM109/pMap8 was routinely grown in 15 L of LB medium supplemented with ampiciline of 100 mg/L of culture medium at 37 °C for 20 h with shaking.

Purification of PfMAP. Pelleted cells (wet weight of about 35 g) collected by centrifugation (5000 rpm for 10 min) were suspended in 110 mL of 30 mM potassium phosphate buffer (pH 7.0). The cells were broken by sonication on ice for 5 min by repeating three times with cooling intervals of 10 min. The homogenized solution was heated in water bath at 100 °C for 5 min, which precipitated the majority of the *E. coli* proteins, leaving *Pf*MAP in the soluble fraction. After heating, the solution was centrifuged at 15 000 rpm for 30 min at 7 °C to remove cell debris and denatured *E. coli* proteins. *Pf*MAP was collected as a precipitate by the addition of ammonium sulfate of 80% saturation. The precipitate was dissolved in 50 mL of 30 mM potassium phosphate buffer (pH 7.0), and the solution was then dialyzed against the same buffer at 25 °C overnight. After removing a small amount of the precipitate by centrifugation at 20 000 rpm for 30 min at 7 °C, the dialyzed sample was applied to a 2.7 cm × 20 cm column of DEAE-Sephacel (Pharmacia) equilibrated with the same buffer. Proteins were separately eluted by a linear gradient with 30 to 1000 mM potassium phosphate buffer (pH 7.0) of each 200 mL. Fractions with MAP activity were collected and concentrated by ultrafiltration through an Amicon PM 10 membrane. Next, a few proteins contaminated in the sample were separated by gel filtration (Superdex200 26/60, Pharmacia) using 30 mM potassium phosphate buffer. Finally, the fractions with MAP activity from the gel filtration were purified by ion exchange chromatography with a linear gradient of 30 to 240 mM of phosphate buffer using SP Sepharose10/26 (Pharmacia). Purified *Pf*MAP showed a single band on SDS−PAGE.

The protein concentration of *Pf*MAP was estimated from the absorbance at the maximum wavelength of 278.5 nm, using $E^{1\%} = 9.63$ with a cell of 1 cm light path length. This value was determined based on the protein assay by the Lowry method using bovine serum albumin as a standard protein.

Assay of Enzymatic Activity. The enzymatic activity was measured in the presence of 1 mM $CoCl_2$ at pH 7.0 by a modification of the methods described by Tsunasawa et al. (*20*) and Ben-Bassat et al. (*16*). L-Met-Ala-Ser-OH (Bachem, Switzerland) was utilized as a substrate. The measurement of the activity was performed at pH 7.0 and 37 °C for 10 min. L-Methionine released by *Pf*MAP was colorimetrically measured by absorbance at 505 nm of the red-colored quinoid formed by the oxidative condensation of 4-amino antipyrine and phenol under coupling reactions with L-amino acid oxidase (from Crotalus adamanteus, Sigma) and peroxidase (from horseradish, Sigma).

Differential Scanning Calorimetry. Differential scanning calorimetry (DSC) was carried out with a differential scanning microcalorimeter, DASM4, equipped with an NEC

[1] Abbreviations: MAP, methionine aminopeptidase; *Pf*MAP, MAP from *P. furiosus*; *Ec*MAP, MAP from *E. coli*; DSC, differential scanning calorimetry.

[2] Tahirov, T. H., Oki, H., Tsukihara, T., Ogasahara, K., Yutani, K., Ogata, K., Izu, Y., Tsunasawa, S., and Kato, I. Crystal structure of methionine aminopeptidase from hyperthermophile, *Pyrococcus furiosus*.

personal computer at a scan rate of 1.0 K/min. Prior to the measurements, the *Pf*MAP solution was dialyzed overnight against a buffer solution used at 4 °C. In all cases, Co^{2+} was not contained in the buffer solutions. Both dialyzed samples and the last dialysis buffer were filtered through a 0.22 μm pore size filter and then degassed in a vacuum. Nitrogen gas in 2.2 kg/cm^2 for DASM4 was supplied to the cells during scanning to minimize degassing during heating. DSC at different heating rates (0.5, 1, and 2 K/min) was carried out with a model 5100 Nano-DSC (Calorimetry Sciences Corp.) with pressure of 2.9 kg/cm^2 to the cells. The protein concentrations under the measurements were 0.7−1.4 mg/mL. The DSC curves were analyzed by the Origin software from MicroCal (Northampton).

CD Spectra. Far- and near-UV CD spectra were recorded on a Jasco J-720 spectropolarimeter equipped with an NEC personal computer. Spectra were accumulated with scanning 16 times at a scan rate of 20 nm/min, using a time constant of 0.25 s. The light path lengths of the cells used were 0.118 mm in the far-UV region and 10 mm in the near-UV region. The protein concentrations under measurement were 1.0−1.3 mg/mL. For calculation of the mean residue ellipticity, [θ], the mean residue weight was taken as 111.3. All the CD measurements were carried out at 25 °C.

Analytical Ultracentrifugation. Sedimentation velocity and sedimentation equilibrium measurements were carried out with a Beckmann Optima mode XL-A at 20 °C. Prior to the measurements, *Pf* MAP was dialyzed against the buffer solution without Co^{2+} at various pHs in the absence or in the presence of KCl over 20 h at 4 °C. The concentrations of *Pf*MAP used for the measurement were 0.7−1.0 mg/mL. The partial specific volume of *Pf*MAP was assumed to be 0.755 cm^3/g from amino acid composition (*24, 25*).

RESULTS

Differential Scanning Calorimetry of PfMAP. The thermal stability of *Pf*MAP was examined by differential scanning calorimetry (DSC). Prior to the DSC measurement, the *Pf*MAP solution was tested as to whether it aggregates at higher temperatures. The protein solutions in concentrations of 0.6−1.5 mg/mL were visibly turbid in the pH range from 4.5 to 9.5 by heating at 130 °C for 5 min in sealed grass tubes. Hence, the DSC of *Pf*MAP was carried out in the acidic and alkaline pH regions far from the isoelectric point of 7.8 of *Pf*MAP estimated by isoelectric focusing. Figure 1 displays the typical heat capacity curves of *Pf*MAP in different pHs at a heating rate of 1 K/min. The curves had a single peak above pH 2.8 (curves 1, 2, and 3 in Figure 1). In the pH region 2.6−1.9, the DSC curves exhibited no excess heat capacity, which is characteristic of the denaturation of a protein, but did exhibit monotonically a temperature dependence of the heat capacity (curves 4 and 5 in Figure 1), suggesting that *Pf*MAP is in the denatured state in its region. However, below pH 1.8, a small peak appeared (curves 6 and 7 in Figure 1). After cooling the heat denatured samples in the calorimetry cell, the repetitive DSC curves were not reproducible, demonstrating that the heat denaturation of *Pf*MAP was not reversible under the conditions used. However, the excess heat capacity curves exhibited the post-transition baselines anticipated for general heat denaturation of a protein, resulting in that the heat

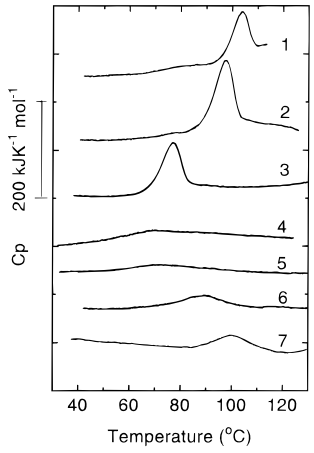

FIGURE 1: Typical heat capacity curves of *Pf*MAP at different pHs. The measurements were performed at heating rate of 1 K/min using DASM4. The buffer solution used was 20 mM glycine-HCl or 20 mM glycine-KOH. In all cases, Co^{2+} was not contained in the buffer solutions. Curve 1, pH 10.13; 2, pH 3.88; 3, pH 2.99; 4, pH 2.55; 5, pH 2.30; 6, pH 1.62; 7, pH 1.29. pH values of the samples after DSC measurements are given.

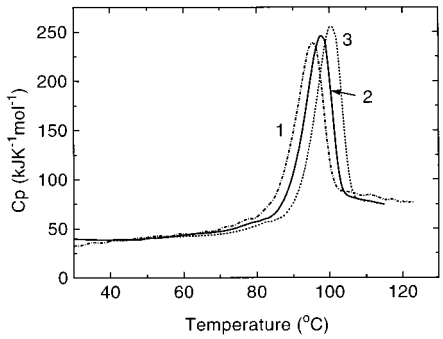

FIGURE 2: Heat capacity curves of *Pf*MAP at different heating rates. Curves 1, 2, and 3 were measured at heating rates of 0.5, 1, and 2 K/min, respectively, at pH 3.78 (20 mM glycine-HCl buffer), using Nano DSC. Each curve has been subtracted the baseline of the buffer solution (20 mM glycine-HCl) scanned at each heating rate. pH values of the samples after DSC measurements are given.

capacity change upon denaturation could be obtained from the difference in the values of the heat capacity (C_p) for the native and denatured states at denaturation temperature.

Figure 2 shows the heat capacity curves of *Pf*MAP at pH 3.78 at different heating rates. The peak temperatures at the heating rates of 0.5 and 2.0 K/min were 2.1 °C lower and 2.7 °C higher, respectively, than that at the heating rate of 1 K/min, suggesting that the heat denaturation of *Pf*MAP at the heating rates of 1 and 2 K/min did not attain equilibrium during heating. The heat denaturation of *Pf*MAP was also irreversible at heating rates of 2 and 0.5 K/min.

pH Dependence of Thermal Stability of PfMAP. Figure 3 shows the pH dependence of the peak temperature (T_m) on the excess heat capacity curves at the heating rate of 1 K/min. T_m values of *Pf*MAP were 100.0 °C at pH 4.0 and over (106.2 °C) boiling point of water at pH 10.2. It was found that the purified *Pf*MAP itself is, indeed, remarkably heat resistant as well as several proteins from hyperthermophiles monitored by calorimetry (*13, 26−31*). T_m decreased with lowering the pH from 4 to 2.8. On the other hand, the peak temperatures for small peaks appearing below pH 1.8 shifted to higher temperature with lowering of the pH.

As shown in Figures 1 and 2, since the complete endothermic transitions for the denaturation were obtained,

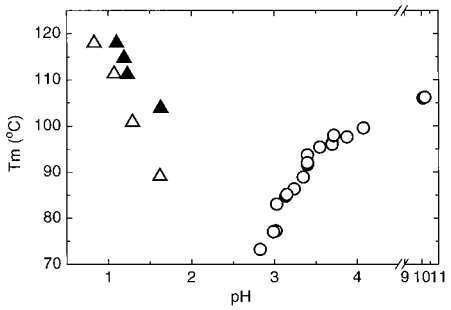

FIGURE 3: pH dependence of the denaturation temperature (T_m) of *Pf*MAP. Heating rate was 1 K/min in 20 mM glycine-HCl or 20 mM glycine-KOH buffer using DASM4. T_m is the peak temperature on DSC curve. (○) In the absence of KCl above pH 2.8; (△) in the absence of KCl below pH 1.9; (▲) in the presence of 50 mM KCl below pH 1.9.

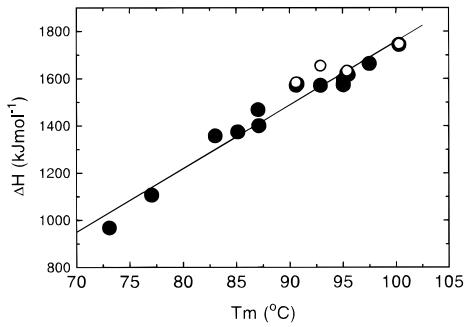

FIGURE 4: Temperature dependence of denaturation enthalpy of *Pf*MAP. T_m is the peak temperature on DSC curves at various pHs. Denaturation enthalpy (ΔH) was calculated from the area under the excess heat capacity curves. (●) Heating rate of 1 K/min; (○), heating rates of 0.5 and 2 K/min. The straight line was obtained from a least-squares fit of experimental data points. Heat capacity change (ΔC_p) was evaluated to be 0.82 J K^{-1} g^{-1} from the slope of the line.

where both the pre- and post-transition baselines could be well-defined, we calculated the enthalpy change (ΔH) upon the thermal transition from the area under the excess heat capacity curve. The ΔH values above pH 2.8 measured at a heating rate of 1 K/min linearly increased with increasing T_m (Figure 4). The ΔH values obtained at heating rates of 0.5 and 2 K/min (Figure 2) were overlaid on the linear line obtained at a heating rate of 1 K/min within experimental error (Figure 4).

The major origin of the irreversibility of a heat denaturation of a protein is, in general, supposed to come from aggregation. The aggregation causes the apparent ΔH value to be underestimated, because a protein aggregation is exothermic. In the case of *Pf*MAP, however, we confirmed by analytical centrifugation experiments that *Pf*MAP after heat denaturation was not accompanied by aggregation. Moreover, the fact that the ΔH at heating rates of 0.5 and 2 K/min coincided with that of 1 K/min at the same values of T_m also excludes the occurrence of the aggregation. These results suggest that the ΔH for *Pf*MAP obtained from the DSC could measure the enthalpy change due to heat denaturation, although the heat denaturation of *Pf*MAP did not attain equilibrium at a heating rate of 1 K/min and was not reversible.

Effect of Salts on Thermal Stability of PfMAP. From the high contents of Glu and Lys in *Pf*MAP and the destabilization by reducing pH in the acidic region (Figure 3), we could

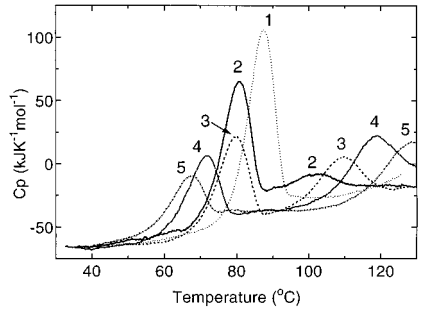

FIGURE 5: Effect of KCl on heat capacity curve of *Pf*MAP at pH 3.2. Heating rate was 1 K/min using DASM4. The buffer solution used for all samples was 20 mM glycine-HCl, pH 3.2. Curve 1 is in the absence of KCl. Curves 2, 3, 4, and 5 are in the presence of 10, 20, 50, and 100 mM KCl, respectively.

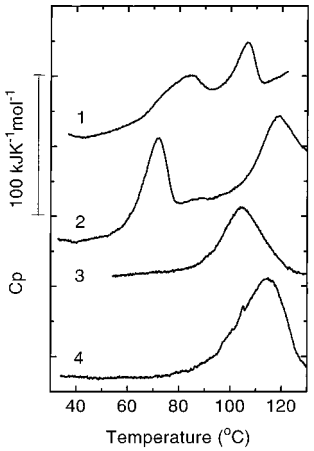

FIGURE 6: Typical heat capacity curves of *Pf*MAP in the presence of 50 mM KCl at various pHs. Heating rate was 1 K/min using DASM4. The buffer solution used for all samples was 20 mM glycine-HCl in the acidic region and glycine-KOH in alkaline pHs. Curve 1, pH 10.00; 2, pH 3.15; 3, pH 1.63; 4, pH 1.19.

postulate the contribution of the electrostatic interactions to the stabilization of *Pf*MAP. We then examined the effect of KCl on the thermal stability of *Pf*MAP. The addition of KCl produced the occurrence of the two peaks clearly separated on the heat capacity curves of *Pf*MAP at pH 3.2. The first peak shifted to lower temperatures with increasing concentration of KCl from 10 to 100 mM, while oppositely, the second one shifted to higher temperatures (Figure 5). To examine whether the separation of the peak by the addition of KCl occurs at another pHs, the DSC curves were measured in the presence of 50 mM KCl at various pHs. The addition of 50 mM KCl also led to the appearance of two peaks in the region above pH 2.8 and in alkaline pH (Figure 6). The presence of 50 mM KCl also induced a small peak over a higher temperature range in the pH region 2.5−1.8, where *Pf*MAP showed no excess heat capacity in the absence of KCl (Figure 1). The temperature of the small peak observed below pH 1.8 transferred to higher temperature in the presence of 50 mM KCl (Figure 3). The DSC curves of *Pf*MAP in the presence of NaCl also exhibited the two peaks as well as those in the presence of KCl (data not shown).

Characterization of the Species Responsible for Each of the Two Peaks on the DSC Curves of PfMAP in the Presence of KCl. To explore the causes of the separation of the peak on the DSC curves of *Pf*MAP in the presence of KCl, the structure of *Pf*MAP was monitored by the far- and near-UV

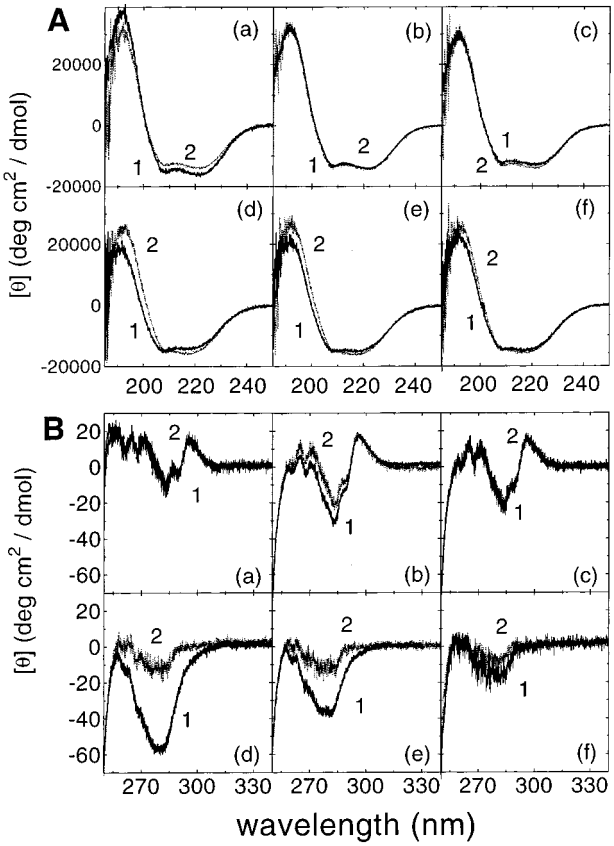

FIGURE 7: CD spectra of *Pf*MAP in the absence and presence of 50 mM KCl at various pHs and 25 °C. 20 mM potassium phosphate buffer was used at neutral pH. 20 mM glycine-HCl and 20 mM glycine-KOH buffers were used in the acidic and alkaline regions, respectively. Far-UV and near-UV CD spectra are displayed in panels A and B, respectively. Curves 1 (solid lines) and 2 (dotted lines) are the spectra in the absence and in the presence of 50 mM KCl, respectively. In panels A and B, respectively, (a) curve 1, pH 10.43; (a) curve 2, pH 10.00; (b) curve 1, pH 7.00; (b) curve 2, pH 6.92; (c) curve 1, pH 3.29; (c) curve 2, pH 3.19; (d) curve 1, pH 2.22; (d) curve 2, pH 2.22; (e) curve 1, pH 1.84; (e) curve 2, pH 1.82; (f) curve 1, pH 1.64; (f) curve 2, pH 1.63.

CD spectra (Figure 7). The far-UV CD spectrum of *Pf*MAP in the native state at pH 7.0 and 25 °C in the absence of KCl was a typical shape for a protein containing a helical structure with a negative peak at 222 nm and a positive peak at 192 nm (column b in Figure 7A). The near-UV CD spectrum of the native *Pf*MAP at pH 7.0 and 25 °C displayed a positive peak at 293 nm and a negative peak at 283 nm with a shoulder at 286 nm (column b in Figure 7B), which are attributed to unique local conformations around aromatic residues, because *Pf*MAP contains a single Trp, 12 Tyr, and eight Phe (*20*). The addition of 50 mM KCl at pHs 7.0 and 3.2 did not change the far- and near-UV CD spectra (columns b and c in Figures 7A and B).

At pH 2.2 in the absence of KCl, in which the excess heat capacity was not observed on the DSC curve (curve 5 in Figure 1), the far-UV CD spectrum above 200 nm was similar to that of the native state at pH 7.0, although the CD value of the peak at 192 nm was reduced (column d in Figure 7A). For the near-UV CD spectra below pH 2.2 in the absence of KCl, the positive peak at 293 nm characteristic for the native state completely disappeared, and the broad trough around 280 nm occurred. The negative CD value of the trough decreased as the pH was lowered (columns d, e, and f in Figure 7B).

In the presence of 50 mM KCl at pHs of 2.2, 1.8, and 1.6, the far-UV CD spectra of *Pf*MAP were similar to that of the native state, except for the decrease in the CD values at 192 nm, indicating that the secondary structure is substantially retained (columns d, e, and f in Figure 7A). In contrast, the tertiary structure of *Pf*MAP was destroyed under these conditions, judging from the near-UV CD spectra with only a small broad trough around 280 nm (columns d, e, and f in Figure 7B). The near-UV CD spectrum in the absence of KCl at pH 1.6 (column f in Figure 7B) was similar to those in the presence of 50 mM KCl at pHs of 2.2, 1.8. The properties of *Pf*MAP in the presence of KCl under strong acidic condition is characteristic of a molten globule with nativelike secondary structure, but disruption of the tertiary structure (*32*−*35*).

Furthermore, we examined the molecular assembly in the absence and in the presence of 50 mM KCl in the acidic region by ultracentrifugation analysis. The apparent molecular weight of *Pf*MAP in 20 mM glycine-HCl buffer, pH 3.2, was estimated to be 30 000 from sedimentation equilibrium experiment. This value is close to the one calculated from amino acid composition (32 740), confirming that *Pf*MAP exists as a monomer in solution at pH 3.2 The sedimentation velocity experiment of *Pf*MAP at pH 3.2 yielded a single symmetrical boundary with an $s^\circ_{20,w}$ of 2.3 S in the absence of 50 mM KCl. In the presence of 50 mM KCl at pH 3.2, the $s^\circ_{20,w}$ value slightly dropped to 2.9 S, and a small amount of the species with greater molecular weight was observed. The sedimentation velocity profile showed two peaks with $s^\circ_{20,w}$ of 3.0 and 5.2 S at pH 2.2 in the absence of KCl, but only one peak of 5.5 S in the presence of 50 mM KCl. At pH 1.9, one major peak with an $s^\circ_{20,w}$ of 5.6 S in the absence of KCl and a single peak with an $s^\circ_{20,w}$ of 7.0 S in the presence of 50 mM KCl were observed. These results reveal that *Pf*MAP is in the associated form below pH 2.2 and that KCl stimulates the molecular assembly of *Pf*MAP.

From the present results, it can be concluded that the small peaks on the DSC curve observed in the high-temperature region above 90 °C in the absence of KCl at strong acid pH (Figure 1) or in the presence of KCl (Figure 6) did not come from the thermal transition of the native state of *Pf*MAP but from the non-native form (molten globule-like assembly form). According to this finding, we can speculate that the first peaks on the DSC curves at pH 3.2 under various concentrations of KCl (Figure 5) arise from the heat denaturation of the native state and the second peak from the melting of the non-native state. This means that the thermal stability of the *Pf*MAP in the native state is reduced by KCl resulting in the decrease of T_m with increasing concentration of KCl, but the conformation in the non-native state is stabilized by KCl.

DISCUSSION

The Irreversibility of Heat Denaturation of PfMAP. The heat denaturation of *Pf*MAP was irreversible in the solvent condition of 20 mM glycine-HCl buffer. The heat denaturation of several proteins from hyperthermophiles monitored by DSC have been reported to be irreversible (*13*, *26*, *28*,

30). The irreversibility of these proteins is suspected to be mainly due to easily formed aggregation at remarkably high temperatures. However, the irreversibility of the heat denaturation for our *Pf*MAP is not supposed to originate only from aggregation, because *Pf*MAP after heating to 125 °C at pH 3.2 by DSC measurement did not aggregate, judging from ultracentrifugation analysis. Pfeil et al. (*36*) have stated that the heat-denatured hyperthermophile ferredoxin does not aggregate, although the denaturation of the ferredoxin is irreversible. One of the rational causes may be heat modification due to deamination of Asn residue, or hydrolysis of peptide bond at Asp residue at high temperature (*37*).

Recently, reversible heat denaturation has been reported on two DNA-binding proteins with small molecular weight from hyperthermophiles: Sac7d (*38*) and Sso7d (*39*). It has been mentioned that the small molecular mass (about 7 kDa) and the measurements in the acidic region far from the isoelectric point result in good reversibility. However, the irreversibility of the heat denaturation is not an inherent property for hyperthermophile proteins with large molecular weight, since we have observed that pyroglutamyl peptidase from *P. furiosus*, a homotetramer with molecular weight of 22 800 per monomer, undergoes the reversible heat denaturation in the acidic region (in preparation). Hyperthermophiles thrive best and can reproduce near 100 °C. This means that a nascent protein polypeptide chain can fold to a mature active form at such high temperature in the cell. There should be suitable conditions in vitro for reversibly refolding, or it may be necessary to help by other factors such as molecular chaperon.

The Features of the Heat Denaturation of PfMAP. The denaturation temperature (T_m) of *Pf*MAP was higher at a rapid heating rate than at a slow rate (Figure 2). This suggests that the rate of the heat denaturation of *Pf*MAP is slower than those of proteins from mesophiles, because the heat denaturation for most mesophile proteins can attain the equilibrium by heating at 1 K/min, and the extraordinary stability of *Pf*MAP depends on the kinetic property of the denaturation. We will report the equilibrium and kinetic study of *Pf*MAP in a following paper.

Thermodynamic analysis of protein stability gives an important insight into the stabilization mechanism of a hyperthmophile protein. The thermodynamic parameters can be obtained for the reversible denaturation. Although the heat denaturation of our *Pf*MAP was not reversible, as stated in a section of Results, the ΔH for *Pf*MAP obtained from DSC was equivalent to the enthalpy change upon heat denaturation. Although the heat denaturation of ferredoxin from a hyperthermophile *T. maritima* is irreversible, the unfolding process has been interpreted thermodynamically (*36*), because the heat denaturation of this protein is not accompanied by further heat-absorbing or heat-releasing processes, indicating the denatured chain does not aggregate. For globular proteins from mesophiles, the linear correlation between ΔH and T_m has been experimentally observed up to about 80 °C, which means no temperature dependence of ΔC_p up to 80 °C (*40*−*45*). However, it has been postulated that the ΔC_p values of proteins become zero at 110 °C regardless of the kind of protein (*40*−*45*), because the C_p in the native state on the excess heat capacity curve linearly increases with increasing temperature, and the C_p in the denatured state is nearly constant over 80 °C. In the case of *Pf*MAP, the linear correlation between ΔH and T_m was prolonged up to 100 °C by experimentally measured data points (Figure 4). In fact, for the DSC curves at pHs where T_m was near 100 °C or over, the C_p value in the denatured state was greater than that in the native state, resulting in that ΔC_p could be directly obtained as the difference in the C_p values of the native and denatured states (Figures 1 and 2). For Sac7d and Sso7d from hyperthermophiles, the linearity is obtained up to 91−97 °C (*38*, *39*). The difference in the C_p values of the native and denatured states of a protein should not disappear at 110 °C.

The ΔC_p for *Pf*MAP was estimated to be 0.82 J K^{-1} g^{-1} from the slope in the linear correlation between ΔH and T_m in the absence of KCl (Figure 4). This value was equivalent to the values obtained directly from individual calorimetric scans at various pHs: for example, 0.79 J K^{-1} g^{-1} at T_m of 87.0 °C at pH 3.2. The ΔC_p value for *Pf*MAP is the upper limit for those of the general globular proteins from mesophiles (*40*, *41*). Because ΔC_p is mainly attributed to the increase in hydrophobic residues exposed upon denaturation (*40*−*45*), the value of ΔC_p for *Pf*MAP suggests that the hydrophobic residues buried in the interior of the molecule are slightly more than those for mesophile proteins. On the other hand, ΔC_p values of Sac7d and Sso7d with small molecule weights from hyperthermophiles are lower than those of mesophile proteins (*38*, *39*). The authors have stated that the reason for the small ΔC_p is that small proteins are unable to form a large hydrophobic core due to their size.

The Molten Globule-Like State of the Hyperthermophilic PfMAP Induced by Salt or Acid. *Pf*MAP exhibited properties (nativelike secondary structure without unique tertiary structure) typical of the molten globule state in the presence of KCl or in the strong acidic region as judged from CD spectra (Figure 7). Change into the molten globule state by salts or the decrease in pH has been reported for some proteins from mesophiles (*32*, *46*) [see the review by Ptitsyn (*35*)]. The molten globule state has been known as an important intermediate in protein-folding pathway (*34*, *35*). The present results indicated that proteins from hyperthermophiles also adopt the molten globule state. The molten globule of *Pf*MAP cooperatively melted depending on the concentration of KCl at a higher temperature than the native state, indicating that the molten globule state for *Pf*MAP is more stable than the native state and its stability is affected by the concentration of KCl. It has been reported that the unfolding of the molten globule state is caused by the increase in electrostatic interaction (*32*, *47*) and also that the stability of the molten globule state is altered by the amino acid substitution (*48*, *49*). The melting by heating of the molten globule state is controversial. Some proteins have no cooperative transition by heating (*50*, *51*), whereas other proteins cooperatively melt accompanied by excess heat capacity (*52*). In the case of *Pf*MAP, the high transition temperature may be arisen from the melting of both the destruction of the collapsed structure and the dissociation of the associated form.

Contribution of Electrostatic Interaction, Ion Pairs, to the Stability of PfMAP. The stability of *Pf*MAP decreased with decreasing pH (Figure 3). Moreover, it was revealed that the native form of *Pf*MAP was destabilized by the addition of KCl (Figure 5). Positive and negative charges on the surface of *Pf*MAP interact with each of the Cl^- and K^+ in

Table 1. Number of Ion Pairs in *Pf*MAP and *Ec*MAP

	Pf MAP[a]	*Ec*MAP[b]
no. of ion pairs within 3 Å	12	8
between 3 and 4 Å	25	8
between 4 and 6 Å	59	41
within 6 Å	96	57
no. of ion pairs per residue within 3 Å	0.04	0.03
between 3 and 4 Å	0.08	0.03
between 4 and 6 Å	0.20	0.16
within 4 Å	0.13	0.06
within 6 Å	0.32	0.21

[a] Ion pairs between the positively and negatively charged side chains were evaluated. The crystal structure of *Pf*MAP was determined by the resolution of 1.75 Å (1xgs.pdb, personal communication from Dr. T. Tahirov et al.). [b] The crystal structure of *Ec*MAP determined by 2.4 Å was taken from Roderick and Matthews (*23*).

the presence of KCl, and negative charges are protonated by lowering the pH in the acidic region, resulting in the perturbation of attractive electrostatic interaction. Thus, our observations indicate an important role of the salt bridge as the predominant force stabilizing *Pf*MAP. The crystal structure of *Pf*MAP has been determined by the resolution of 1.75 Å (1xgs.pdb, personal communication from Dr. T. Tahirov et al.). The three-dimensional structure of *Pf*MAP constitutes two domains: the large catalytic domain and a small domain. The catalytic domain of *Pf*MAP has topological structure similar to *Ec*MAP. The extra insertion sequence of 62 residues compared with *Ec*MAP constitutes the small domain. Several factors contributing to the stability of *Pf*MAP have been suggested from the differences in a comparison of the structure of *Ec*MAP (*23*): one of them is ion pairs. *Pf*MAP contains significantly large number of ion pairs compared with *Ec*MAP. Table 1 summarizes the ion pairs involved in *Pf*MAP and *Ec*MAP. Concerning the ion pairs within a short length of 3 Å, *Pf*MAP includes four extra ion pairs compared with *Ec*MAP. The extra ion pairs in *Pf*MAP are 17Arg-Glu18 (center of helix A), 127Glu-Lys129 (N-terminal of helix D), 171Arg-Asp174 (turn), and a triad of Lys141-Glu138-Arg142 (C-terminal of helix D). The accessible surface areas (ASA) of the residues were 6% for Arg17, 46% for Glu18, 34% for Glu127, 15% for Lys129, 46% for Arg171, 13% for Asp174, 62% for Lys141, 22% for Glu138, and 27% for Arg142. Three of the ion pairs were intrahelical. This suggests that intrahelical electrostatic interactions through the Glu^{-}-Lys^{+} (or Arg^{+}) salt bridge contribute to helix stabilization in *Pf*MAP as reported in the model peptides (*53*, *54*). When compared with sequence alignments of eighteen kinds of MAPs from various sources (personal communication from Dr. T. Tahirov et al.), other MAPs do not have ion pairs at positions corresponding to 127Glu-Lys129, 171Arg-Asp174, and a triad of Lys141-Glu138-Arg142 in *Pf*MAP, but only a single ion pair corresponding to 17Arg-Glu18 in *Pf*MAP is detected in a eukaryotic-type MAP from a hyperthermophile, *Methanococcus jannaschii*. From these findings, it is likely that the three kinds of single ion pair and the triad ion pair are crucial candidates as determinants for the superior thermostability of *Pf*MAP. Moreover, *Pf*MAP includes 17 more ion pairs in the length of 3−4 Å and 18 more pairs in the length of 4−6 Å than *Ec*MAP (Table 1). Some of the additional long-range ion pairs should be also important for the stabilization of *Pf*MAP, since a long-range salt bridge separated by 5−6 Å has been reported to contribute to the stabilization of barnase (*55*).

The importance of electrostatic interaction in the high thermostability of hyperthermophile proteins has been experimentally proven using mutant D-glyceraldehyde 3-phosphate dehydrogenase, which is replaced charged residues by noncharged ones (*56*). The denaturation temperature of rubredoxin is 42 °C lower at pH 2 than at pH 7, suggesting stabilization by electrostatic interaction (*57*). On the other hand, the increase of ionic strength has enhanced the thermostabilities of hyperthermophile rubredoxin (*57*) and TATA-box binding protein (*13*). DeDecker et al. (*13*) have mentioned that the increased thermostability of the TATA-box binding protein at a higher concentration of salt argues against electrostatic interactions as predominant stabilizing forces.

For general proteins from mesophiles, the salt bridges have been reported to be a stabilizing factor for proteins (*58*−*63*), contrary, to become a destabilizing factor (*64*). The crystal structures of hyperthermophile proteins have revealed a significant increase in ion pairs on the surface of the molecules (*7*, *9*−*13*). Hyperthermophile proteins can be used as a model system for elucidating the role of a salt bridge in stabilizing a protein. We have examined the contribution of the salt bridges to the stability of *Pf*MAP using the engineered *Pf*MAPs which delete ion pairs.

ACKNOWLEDGMENT

We greatly thank Dr. Haruki Nakamura (Biological Engineering Research Institute) for valuable discussion on the role of salt bridges in stabilizing the protein.

REFERENCES

1. Stetter, K. O. (1982) *Nature 300*, 258−260.
2. Stetter, K. O., Fiala, G., Huber, G., Huber, R., and Segerer, A. (1990) *FEMS Microbiol. Rev. 75*, 117−124.
3. Adams, M. W. W. (1993) *Annu. Rev. Microbiol. 47*, 627−658.
4. Adams, M. W. W. (1994) *FEMS Microbiol. Rev. 15*, 261−277.
5. Woese, C. R., Kandler, O., and Wheelis, M. L. (1990) *Proc. Natl. Acad. Sci. U.S.A. 87*, 4576−4579.
6. Gros, F., and Tocchini-Valentini, G. P. (1994) *Nature 369*, 11−12.
7. Day, M., W., Hsu, B. T., Joshua-Tor, L., Park, J.-B., Zhou, Z. H., Adams, M. W. W., and Rees, D. C. (1992) *Protein Sci. 1*, 1494−1507.
8. Russell, R. J. M., Hough, D. W., Danson, M. J., and Taylor, G. L. (1994) *Structure 2*, 1157−1167.
9. Yip, K. S. P., Stillman, T. J., Britton, K. L., Artymiuk, P. J., Baker, P. J., Sedelnikova, S. E., Engel, P. C., Pasquo, A., Chiaraluce, R., Consalvi, V., Scandurra, R., and Rice, D. W. (1995) *Structure 3*, 1147−1158.
10. Korndorfer, I., Steipe, B., Huber, R., Tomschy, A., and Jaenicke, R. (1995) *J. Mol. Biol. 246*, 511−521.
11. Chan, M. K., Mukund, S., Kletzin, A., Adams, M. W. W., and Rees, D. C. (1995) *Science 267*, 1463−1469.
12. Hennig, M., Darimont, B., Sterner, R., Kirschner, K., and Jansonius, J. N. (1995) *Structure, 3*, 1295−1305.
13. DeDecker, B. S. O'Brien, R., Fleming., P. J., Geiger, J. H., Jackson, S. P., and Sigler, P. B. (1996) *J. Mol. Biol. 264*, 1072−1084.
14. Knapp, S., DeVos, W. M., Rice, D., and Ladenstein, R. (1997) *J. Mol. Biol. 267*, 916−932.
15. Fiala, G., and Stetter, K. O. (1986) *Arch. Microbiol. 145*, 56−61.

16. Ben-Bassat, A., Bauer, K., Chang., S.-Y., Myambo, K., Boosman, A., and Chang, S. (1987) *J. Bacteriol. 169*, 751−757.
17. Miller, C,. G., Strauch, K. L., Kukral, A. M., Miller, J. L., Wingfield, P. T., Mazzei, G. J., Werlen., R. C., Graber, P., and Movva, N. R. (1987) *Proc. Natl. Acad. Sci. U.S.A. 84*, 2718−2722.
18. Arfin, S. M., Kendall, R. L., Hall, L., Weaver, L. H., Stewart, A. E., Matthews, B. W., and Bradshaw, R. A. (1995) *Proc. Natl. Acad. Sci. U.S.A. 92*, 7714−7718.
19. Li, X. and Chang, Y.-H. (1995). *Proc. Natl. Acad. Sci. U.S.A. 92*, 12357−12361.
20. Tsunasawa, S., Izu, Y., Miyagi, M., and Kato, I. (1997) *J. Biochem. 122*, 843−850.
21. Perutz, M. F., and Raidt, H. (1975) *Nature, 255*, 256−259.
22. Perutz, M. F. (1978) *Science 201*, 1187−1191.
23. Roderick, S. L., and Matthews, B. W. (1993) *Biochemistry, 32*, 3907−3912.
24. McMeekin, T. L., and Marshall, K. (1982) *Science 116*, 142−145.
25. Perkins, S. J. (1986) *Eur. J. Biochem. 157*, 169.
26. Wrba, A., Schweiger, A., Schultes, V., Jaenicke, R., and Zavodszky, P. (1990) *Biochemistry 29*, 7584−7592.
27. Klump, H., Ruggiero, J., Kessel, M., Park, J.-B., Adams, M. W. W., and Robb, F. (1992) *J. Biol. Chem. 267*, 22681−22685.
28. Laderman, K. A., Davis, B. R., Krutzsch, H. C., Lewis, M. S., Griko, Y. V., Privalov, P. L., and Anfinsen, C. B. (1993) *J. Biol. Chem., 268*, 24394−24401.
29. Davies, G. J., Gamblin, S. J., Littlechild, J. A., and Watson, H. C. (1993) *Proteins: Struct., Funct., Genet. 15*, 283−289.
30. Klump, H. H., Adams, M. W. W., and Robb, F. T. (1994) *Pure Appl. Chem. 66*, 485−489.
31. Jaenicke, R., Schurig, H., Beaucamp, N., and Ostendorp, R. (1996) *Adv. Protein Chem. 48*, 181−269.
32. Ohgushi, M., and Wada, A. (1983) *FEBS Lett. 164*, 21−24.
33. Ohgushi, M., and Wada, A. (1984) *Adv. Biophys. 18*, 75−90.
34. Kuwajima, K. (1989) *Proteins: Struct., Funct. Genet. 6*, 87−103.
35. Ptitsyn, O. B. (1992). in *Protein Folding* (Creighton, T. E., Ed.) pp 243−300, W. H. Freeman and Company, New York.
36. Pfeil, W., Gesierich, U., Kleemann, G. R., and Sterner, R. (1997) *J. Mol. Biol. 272*, 591−596.
37. Ahern, T. J., and Klibanov, A. M. (1985) *Science 228*, 1280−1284.
38. McCrary, B. S., Edmondson, S. P., and Shriver, J. W. (1996) *J. Mol. Biol. 264*, 784−805.
39. Knapp, S., Karshikoff, A., Berndt, K. D., Christova, P. Atanasov, B., and Ladenstein, R. (1996) *J. Mol. Biol. 264*, 1132−1144.
40. Privalov, P. L., and Khechinashvili, N. N. (1974). *J. Mol. Biol. 86*, 665−684.
41. Privalov, P. L (1979) *Adv. Protein Chem. 33*, 167−241.
42. Privalov, P. L., and Gill, S. J. (1988) *Adv. Protein Chem. 39*, 191−234.
43. Privalov, P. L., and Makhatadze, G. I. (1990) *J. Mol. Biol. 213*, 385−391.
44. Makhatadze, G. I. *Adv. Protein Chem*. (1995) *47*, 308−425.
45. Murphy, K. P., and Freire, E. (1992) *Adv. Protein Chem. 43*, 313−361.
46. Fink, A. L., Calciano, L. J., Goto, Y., and Palleros, D. R. (1991) in *Conformations and Forces in Protein Folding* (Nall, B. T., and Dill, K. A., Eds.) pp 169−174, AAAS, Washington, D. C.
47. Wong, K.-P., and Hamlin, L. M. (1974) *Biochemistry 13*, 2678−2683.
48. Uchiyama, H., Perez-Prat, E. M., Watanabe, K., Kumagai, I., and Kuwajima, K. (1995) *Protein Eng. 8*, 1153−1161.
49. Ogasahara, K., and Yutani, K. (1997) *Biochemistry 36*, 932−940.
50. Pfeil, W., Bychkova, V. E., and Ptitsyn, O. B. (1986) *FEBS Lett. 198*, 287−291.
51. Yutani, K., Ogasahara, K., and Kuwajima, K. (1992) *J. Mol. Biol. 228*, 347−350.
52. Potekhin, S. A., and Pfeil, W. (1989) *Biophys. Chem. 34*, 55−62.
53. Marqusee, S., and Baldwin, R. L. (1987). *Proc. Natl. Acad. Sci. U.S.A. 84*, 8898−8902.
54. Huyghues-Despointes, B. M. P., Scholtz, J. M., and Baldwin, R. (1993) *Protein Sci. 2*, 80−85.
55. Serrano, L., Horovitz, A., Avron, B., Bycroft, M., and Fersht, A. R. (1990) *Biochemistry 29*, 9434−9352.
56. Tomschy, A., Bohm, G., and Jaenicke, R. (1994) *Protein Eng. 7*, 1471−1478.
57. Cavagnero, S., Zhou, Z. H., Adams, M. W. W., and Chan, S. I. (1995) *Biochemistry 34*, 9865−9873.
58. Albert, T., Dao-pin, S., Nye, J. A., Muchmore, D. C., and Matthews, B. W. (1987) *Biochemistry 26*, 3754−3758.
59. Anderson, D. E., Becktel, W. J., and Dahlquist, F. W. (1990) *Biochemistry 29*, 2403−2408.
60. Dao-pin, S., Sauer, U., Nicholson, H., and Matthews, B. W. (1991) *Biochemistry 30*, 7142−7153.
61. Nicholson, H., Becktel, W. J., and Matthews, B. W. (1988) *Nature 336*, 651−656.
62. Waldburger, C. D., Schildbach, J. F., and Sauer, R. T. (1995) *Nature Struct. Biology, 2*, 122−128.
63. Nakamura, H. (1996) *Q. Rev. Biophys. 29*, 1−90.
64. Milla, M. E., Brown, B. M., and Sauer, R. T. (1994) *Nat. Struct. Biol. 1*, 518−523.

BI973172Q